LBL-21235
Preprint

Submitted to Metallugical
Transactions

MECHANICAL BEHAVIOR OF ALUMINUM-LITHIUM ALLOYS AT CRYOGENIC TEMPERATURES

J. Glazer, S.L. Verzasconi,
R.R. Sawtell, and J.W. Morris,Jr.

March 1986

Lawrence Berkeley Laboratory
University of California
Berkeley, California 94720

Prepared for the U.S. Department of Energy
under Contract DE-AC03-76SF00098

Center for Advanced Materials

DISCLAIMER

Mechanical Behavior of Aluminum-Lithium Alloys at Cryogenic Temperatures

J. Glazer, S. L. Verzasconi, R. R. Sawtell and J. W. Morris, Jr.
Center for Advanced Materials,
Lawrence Berkeley Laboratory, and
Dept. of Materials Science and Mineral Engineering,
University of California, Berkeley

Abstract

The cryogenic mechanical properties of aluminum-lithium alloys are of interest because these alloys are attractive candidate materials for cryogenic tankage. Previous work indicates that the strength-toughness relationship for alloy 2090-T81 (Al-2.7Cu-2.2Li-0.12Zr by weight) improves significantly as temperature decreases. The subject of this investigation is the mechanism of this improvement. Deformation behavior was studied since the fracture mode did not change with temperature. Tensile failures in 2090-T81 and -T4 occur at plastic instability. In contrast, in the binary aluminum-lithium alloy studied here they occur well before plastic instability. For all three materials, the strain hardening rate in the longitudinal direction increases as temperature decreases. This increase is associated with an improvement in tensile elongation at low temperatures. In alloy 2090-T4, these results correlate with a decrease in planar slip at low temperatures. The improved toughness at low temperatures is believed to be due to increased stable deformation prior to fracture.

Introduction

The cryogenic properties of low-density structural materials have acquired considerable importance because of their current and potential uses in space vehicles. For example, the proposed hypersonic and transatmospheric vehicles are expected to use cryogenic fuels such as liquid hydrogen. The large quantity of fuel required to power these vehicles suggests that the cryogenic fuel tank will be structural. Applications of this sort have spurred interest in the cryogenic properties of high-strength aluminum alloys. Although mechanical property data exist for a number of aluminum alloys, to date there has been little work aimed at understanding the mechanisms that control mechanical behavior at cryogenic temperatures.

Aluminum-lithium alloys are attractive for cryogenic tankage because they have both lower densities and higher elastic moduli than the aluminum alloys currently used in these applications, such as the Al-Cu alloy 2219-T87, from which the cryogenic external tank of the space shuttle is constructed. In addition, previous work has indicated that at low temperatures aluminum-lithium alloys display improved toughness and an improved strength-toughness relationship in the L and LT directions [1-3]. The most extensively studied alloy is alloy 2090-T81, of nominal composition Al-2.7Cu-2.2Li-0.12Zr in weight

percent. The cryogenic mechanical properties of alloy 2090-T81 have been characterized [1,2] and are summarized below.

The most striking feature of the low temperature behavior of alloy 2090-T81 is that the yield strength, ultimate tensile strength, elongation and fracture toughness in both the L and LT directions *increase* as temperature *decreases*. Although some other aluminum alloys, including 2219-T87, display this behavior [4], 2090-T81 alloy shows a significantly greater improvement in mechanical properties. The improvement in the strength-toughness relationship with decreasing temperature is illustrated in Figure 1. Similar data for 2219-T87 alloy is included for comparison [5-7]. At 4 K, 2090-T81 plate has a strength-toughness combination that is superior to that obtained to date for any other aluminum alloy. In addition, the tensile elongation in the longitudinal direction increases approximately 60% between room temperature and 4 K. The mechanisms responsible for the variation in mechanical properties with temperature are not currently understood and are the subject of this investigation.

Because dramatic changes in fracture toughness between room and cryogenic temperatures in other systems are usually associated with significant changes in the fracture mode, this possibility was examined first. However, as illustrated by figure 2, decreasing the temperature did not alter the fracture mode or morphology [1]. More recently, Dorward [2] has suggested that the improvement in the fracture toughness of 2090-T8 alloy at low temperature is due to increased short-transverse delamination (splitting in the plane of the plate). Dorward found that the fracture toughness in the S-L orientation decreased slightly at low temperature, which could promote delamination. To test this observation for the present case, the fracture surfaces of the specimens described in reference [1] were specifically examined for increased cracking perpendicular to the fracture surface; however, no qualitative difference was observed.

Since there is no clear change in the fracture behavior at low temperature, the study described here focuses on the variation of deformation behavior with temperature. To simplify experimentation, only tensile deformation was examined. Strain hardening rate behavior, important to formability in general as well as to tensile elongation, is used as a tool to characterize the progress of deformation. At this stage, the results of this work bear primarily on the mechanisms that control elongation at low temperatures. These results are important in their own right, although the eventual purpose of this work is to understand the mechanisms controlling low-temperature toughness.

Experimental Procedures

To provide a greater range of behavior, the study was broadened to include a total of three materials and conditions: (1) 2090-T81, from the same lot of 12.7 mm (0.5 in) plate as reference 1, (2) 2090-T4, prepared by a solution treatment of 2090-T81 at 550°C for 30 minutes followed by a cold water quench and natural aging, and (3) a pseudo-binary alloy, Al-2.4Li-0.1Zr by weight, received as 12.7 mm (0.5 in) plate hot-rolled from an 11 kg (25 lb) ingot, solution treated at 555°C for one hour, cold water quenched, stretched 2%

in tension and aged to peak strength. The actual chemical composition of the 2090 alloy plate, as determined by atomic emission (Cu) and atomic absorption spectroscopy (balance), is Al-2.86Cu-2.05Li-0.12Zr in weight percent. Levels of Fe, Si, Mg, Mn, and Ti were all 0.02 weight percent or less.

Longitudinally oriented flat tensile specimens 3.2 mm (0.125 in) thick were taken from the plates at quarter-thickness. The reduced section of the specimen was approximately 41 mm (1.6 in) long and 9.5 mm (0.375 in) wide. The specimens were mechanically polished to 0.05 μm before testing to facilitate observation of slip line patterns on the surface. After deformation, slices parallel to the rolling plane were removed for transmission electron microscopic (TEM) examination. TEM examination of the specimens was performed using a Philips EM 301 at an operating voltage of 100 kV. Samples were prepared by jet polishing at -30°C at 12V in a 3:1 mixture of methanol and nitric acid. Tensile tests were conducted at three temperatures: room temperature (~298 K), liquid nitrogen (77 K), and liquid helium (4 K). Because some tests were conducted at cryogenic temperatures, a relatively slow strain rate of 8×10^{-5} s^{-1} was selected to allow heat generated by deformation to dissipate. Elongation was measured over a 2.54 cm (1 in) gauge. So that it would be possible to follow the development of the deformation substructure, some tests were interrupted at predetermined engineering strains.

Tensile behavior was characterized using the strain hardening rate, $d\sigma/d\varepsilon$, where σ and ε are the true stress and true strain, respectively. For specimens that exhibited a load drop before failure, the curves were analyzed only up to the peak load, since the true stress cannot be calculated after deformation begins to localize. Errors in load-stroke measurements were corrected using the machine compliance and the elongation in the gauge determined after testing. Instantaneous strain hardening rates were calculated using a five-point fit and smoothed.

Results

The tensile properties of the three materials examined at each test temperature are tabulated in Table I.* The corresponding true stress - true strain curves are shown in figure 3. All curves are cut off at peak load although some of the specimens showed necking-type behavior (2090-T81: 298 K; 2090-T4: 298 K, 77 K). Note that the elongation and stress at a given strain increase as temperature decreases. An apparent exception to this trend was that 2090-T4 had a lower elongation at 4 K than at 77 K; however, only one specimen was tested at 4 K. The engineering stress-strain curves at 4 K showed sharp serrations that approached 70 MPa (10 ksi) in magnitude near failure. These serrations are typical of metals deformed in displacement control at extremely low absolute

* It should be noted that there is a large variation in strength through the thickness of the 2090-T81 plate. The strengths reported here for specimens taken at quarter-thickness are about 15% lower than those reported in reference 1 for specimens taken at mid-thickness. For other aluminum-lithium alloys, this difference has been attributed to texture variations through the thickness of the plate [8,9].

temperatures and are due to adiabatic heating [10,11]. The true stress-strain curves shown in figure 3 were plotted using stresses measured at the peaks of the serrations.

The potential failure modes in fracture tests can be classified as either deformation-controlled or fracture-controlled. The variation in mechanical properties with temperature is determined by the temperature sensitivity of the relevant microstructure-property relation. In the fracture-controlled case, failure occurs when a critical stress or strain is reached, and improved toughness should correspond to changes in the fracture mode. As mentioned in the introduction, no such change was observed in 2090-T81. Due to their much lower strength, the fracture toughnesses of the 2090-T4 alloy and the pseudobinary alloy were not measured; however, the fracture behavior seems to follow a similar trend with temperature. In the deformation-controlled case, the proximate cause of failure is the geometric instability that occurs when the strain hardening rate $d\sigma/d\varepsilon$ drops below the true stress. In this instance, both the substructure that develops during deformation and the strain hardening rate should vary with temperature. Accordingly, both of these features of the deformation behavior were examined.

Figures 4, 5 and 6 compare the true stress and strain hardening rate as a function of true strain. The results of these calculations can be used to distinguish between cases of premature fracture (failure at σ significantly less than $d\sigma/d\varepsilon$) and failures due to macroscopic geometric instabilities (failure at $\sigma \sim d\sigma/d\varepsilon$). Figure 4 shows that 2090-T81 fails in tension at all three temperatures when σ is approximately equal to $d\sigma/d\varepsilon$, despite the fact that only at room temperature did a gradual load drop occur prior to failure. Clearly, failure occurs due to geometric instability and not due to a premature (brittle) fracture. In view of the rather brittle appearance of the fracture, this result is quite surprising. Figure 5 illustrates the opposite behavior in the binary alloy; at both temperatures, early fracture occurred when the strain hardening rate was well above the true stress. The 2090-T4 specimens appeared to exhibit an intermediate behavior, illustrated in figure 6. At all three temperatures, failure occurred when the strain hardening rate dropped below the true stress. However, the strain hardening rate did not drop smoothly with strain; in each case, there was a critical strain at which the strain hardening rate began to decrease quickly, leading rapidly to failure. The amount of strain over which this drop occurs is significant; it was generally 2 to 3 percent. The reason for the sudden drop is still under study; however, it may be a manifestation of the inhomogeneity of deformation within the specimen.

Since elongation is controlled by the magnitude of the strain hardening rate relative to the true stress, the strain hardening rates as a function of true strain were examined for consistent trends with microstructure and temper. Comparison of the strain hardening rates for the two 2090 alloy tempers (same composition) and between the binary alloy and 2090-T4 (similar precipitate distribution) did not indicate a clear relationship. However, comparison of the strain hardening rates as a function of temperature for each alloy and temper, as in figure 7, shows that the strain hardening rate increases as temperature decreases. This increase correlates with the improved elongations measured at lower temperatures. Initial TEM studies of deformed material suggest that the increased strain hardening rate exhibited at low temperatures is a consequence of more homogeneous

deformation. Figure 8 compares the dislocation structure of 2090-T4 after 8% engineering strain at room temperature and 77 K. At room temperature some planar slip has occurred; whereas at 77 K, when the strain hardening rate is higher, the dislocations are tangled and uniformly distributed.

Discussion

Although it is considered "typical" for yield strength to increase and fracture toughness to decrease as temperature decreases from room temperature, the increase in fracture toughness observed for 2090-T81 is not unique. The effect of temperature on the strength-toughness relationship of aluminum alloys varies widely; it may improve, deteriorate or be almost unaffected [4, 12-14]. Unfortunately, there is little microstructural or fractographic evidence to correlate with the mechanical properties data available in the literature. Furthermore, it is difficult to compare much of the 'toughness' data because it is in the form of notched tensile or tear test results. The effect of temperature on tensile elongation also varies.

Because both the toughness and elongation of alloy 2090-T81 improve with decreasing temperature while the fracture mode remains unchanged, this study focusses on the effect of cryogenic temperatures on deformation behavior. The strain hardening rate, $d\sigma/d\varepsilon$, is used to characterize tensile failures. In all three materials the higher strain hardening rates maintained at low temperatures are associated with increased tensile elongation. Although the failure criterion is unclear, this statement is true even for the binary alloy, which fractured prematurely at both test temperatures. For both 2090 tempers, this improvement is clearly because geometric instability is deferred. TEM micrographs of the substructure that develops in 2090-T4 during deformation (see figure 8) indicate that deformation is more homogeneous at low temperatures. Similar observations have been made for α-Fe [15]. Apparently, planar slip decreases the ability of the material to maintain the high strain hardening rate needed to continue stable elongation. While planar slip has long been associated with poor ductility in aluminum-lithium alloys [8,16], these results suggest that its negative influence may be due to its effect on the strain hardening rate rather than to, for instance, increased stress concentrations at grain boundaries.

The results of these experiments suggest that the improved fracture toughness at cryogenic temperatures may be a consequence of increased stable deformation prior to fracture. There are some relevant observations in the literature. It is well-established that fracture in high-strength alloys can occur along planar slip bands under certain conditions [17,18]. A number of studies of both binary and ternary aluminum-lithium alloys have concluded that fracture occurs partially along planar slip bands [8,16]. Koss and Chan [17] modeled fracture along slip bands and concluded that once a crack with a coplanar slip band has formed, slip is restricted in the plane of the slip band, creating large stresses perpendicular to the crack. These stresses lead to deformation normal to the crack front, resulting in a jagged fracture surface that is cleavage-like in appearance. Failures of this sort occur in aluminum-lithium alloys and are especially prevalent in binary aluminum-lithium alloys, supporting the idea that localization of slip may play an important role in the fracture process.

Two parameters that are often used in the forming literature to roughly characterize the forming behavior of metals are the strain hardening exponent, n, and an anisotropy factor, r, defined by the equations

$$\sigma = k\varepsilon^n \quad (1)$$

$$r = \varepsilon_w/\varepsilon_t, \quad (2)$$

where k is a constant and the ε are the true strains along the tensile axis and in the width and thickness directions, respectively. Although neither of these parameters is constant for a non-ideal material, the approximate value still provides some information. For 2090-T81 and -T4, the n-values were approximately 0.1-0.2 and 0.3-0.4, respectively. Values of n for aluminum alloys are generally in this range. Like the strain hardening rates, the n-values increased with decreasing temperature. The r-values for both 2090 tempers were between 0.1 and 0.2, indicating that the strain in the ST direction was much greater than the strain in the LT direction. For an isotropic material, the r-value is unity; these values are quite low even for a wrought aluminum alloy and probably reflect the strong texture of the material.

Conclusions

In the L and LT directions, the yield strength, ultimate tensile strength, elongation and fracture toughness of 2090-T81 increases as temperature decreases. The fracture mode is apparently unchanged by the testing temperature. Tensile failures in 2090-T81 occur when plastic instability occurs. For alloys 2090-T4 and Al-2.4Li-0.1Zr, the ultimate tensile strength and tensile elongation similarly increase as temperature decreases. Tensile failures of alloy 2090-T4, as for alloy 2090-T81, occur when the plastic instability criterion is satisfied. However, in the binary aluminum-lithium alloy premature tensile failure occurred at both room temperature and at 77 K. In all three materials, the strain hardening rate in the longitudinal direction increases as temperature decreases, with a concomitant improvement in elongation. Preliminary TEM studies suggest that the increased strain hardening rate is associated with more homogenous plastic deformation. The decrease in slip planarity thus improves ductility through the deformation behavior rather than through fracture behavior. The improved toughness of alloy 2090-T81 at low temperatures is believed to be due to increased stable deformation prior to fracture.

Acknowledgment

The authors thank the Aluminum Corporation of America for providing the materials used in these experiments. This study was jointly supported by a grant from the Aluminum Company of America and the Director, Office of Energy Research, Office of Basic Energy Science, Material Sciences Division of the U.S. Department of Energy under Contract No. DE-AC03-76SF00098. J. Glazer is supported by an AT&T Bell Laboratories Fellowship.

References

1. J. Glazer, S.L. Verzasconi, E.N.C. Dalder, W. Yu, R.A. Emigh, R.O. Ritchie and J.W. Morris, Jr.: *Adv. Cryo. Eng.*, 1986, vol. 32, p. 397.
2. D. Webster: in *Aluminum-Lithium Alloys III*, 1986, The Institute of Metals, London, p. 602.
3. R.C. Dorward: *Scripta Met.*, 1986, vol. 20, p. 1379.
4. F.G. Nelson and J.G. Kaufman: in Fracture Toughness Testing at Cryogenic Temperatures, ASTM STP 496, 1971, p. 27.
5. J.G. Kaufman, F.G. Nelson, and E.W. Johnson: *Adv. Cryo. Eng.*, 1963, vol.8, p. 661.
6. J.G. Kaufman and M. Holt: *Adv. Cryo Eng.*, 1965, vol. 10, p. 77.
7. C. Fiftal, NBS/DOE Report on Cryogenic Structural Materials for Superconducting Magnets, 1978, vol. 1.
8. P.J. Gregson and H.M. Flower: *Acta Metall.*, 1985, vol. 33, p. 527.
9. M. Peters, J. Eschweiler and K. Welpman: *Scripta Metall.*, 1986, vol. 20, p. 259.
10. R.L. Tobler and R.P. Reed: in NBSIR 81-1645, 1981, National Bureau of Standards, Boulder, CO, p. 185.
11. D.T. Read and R.P. Reed: *Adv. Cryo. Eng.*, 1980, vol. 26, p. 91.
12. K.A. Warren and R.P. Reed: NBS Monograph 63, US Dept. of Commerce, 1963.
13. J.L. Christian and J.F. Watson: *Adv. Cryo. Eng.*, 1961, vol. 6, p. 604.
14. J.L. Christian and J.F. Watson: *Adv. Cryo. Eng.*, 1961, vol. 6, p. 490.
15. R.J. McElroy and Z.C. Szkopiak, *Intl. Metall. Reviews*, 1972, vol. 17, p. 175.
16. W.S. Miller, M.P. Thomas, D.J. Lloyd and D. Creber: in *Aluminum-Lithium Alloys III*, 1986, The Institute of Metals, London, p. 584.
17. D.A. Koss and K.S. Chan: *Acta Metall.*, 1980, vol. 28, p. 1245.
18. D.A. Ryder and R.E. Vian: *J. Inst. Met.*, 1961-1962, vol. 90, p. 383.

Table I. Tensile properties as a function of temperature

Material	T (K)	σ_y MPa (ksi)	σ_{UTS} MPa (ksi)	% elong.
2090-T81	298	455 (66)	490 (71)	6
	77	535 (78)	625 (91)	14
	4	535 (78)	650 (95)	20
2090-T4	298	120 (17)	270 (39)	19
	77	155 (23)	350 (51)	29
	4	190 (28)	435 (63)	25
Al-2.4Li-0.1Zr	298	275 (40)	345 (50)	3
	77	270 (39)	420 (61)	11

Figure Captions

Figure 1. Yield strength- fracture toughness combination as a function of temperature for 2090-T81 alloy. The hatched region represents the range of strength-toughness combinations for typical aerospace aluminum alloys. Data for alloy 2219-T87 as a function of temperature are shown for comparison. (After ref. 1)

Figure 2. Scanning electron micrographs of fracture surfaces of J_{Ic} specimens broken at each test temperature. Note that the fracture mode appears to be unchanged. (From ref. 1)

Figure 3. Effect of temperature on true stress-true strain curves for the three materials.

Figure 4. True stress and strain hardening rate (shr) plotted as a function of true strain for alloy 2090-T81 for each test temperature. The true stress and the strain hardening rate (both plotted on the vertical axis) are measured in the same units.

Figure 5. True stress and strain hardening rate (shr) plotted as a function of true strain for Al-2.4Li-0.1Zr alloy as a function of temperature.

Figure 6. True stress and strain hardening rate (shr) plotted as a function of true strain for alloy 2090-T4 for each test temperature.

Figure 7. Effect of temperature on strain hardening rate plotted as a function of true strain for the three materials.

Figure 8. Transmission electron micrograph of alloy 2090-T4 deformed 8% in tension (top) at room temperature, (bottom) at 77 K. Examples of planar slip are arrowed in the upper micrograph.

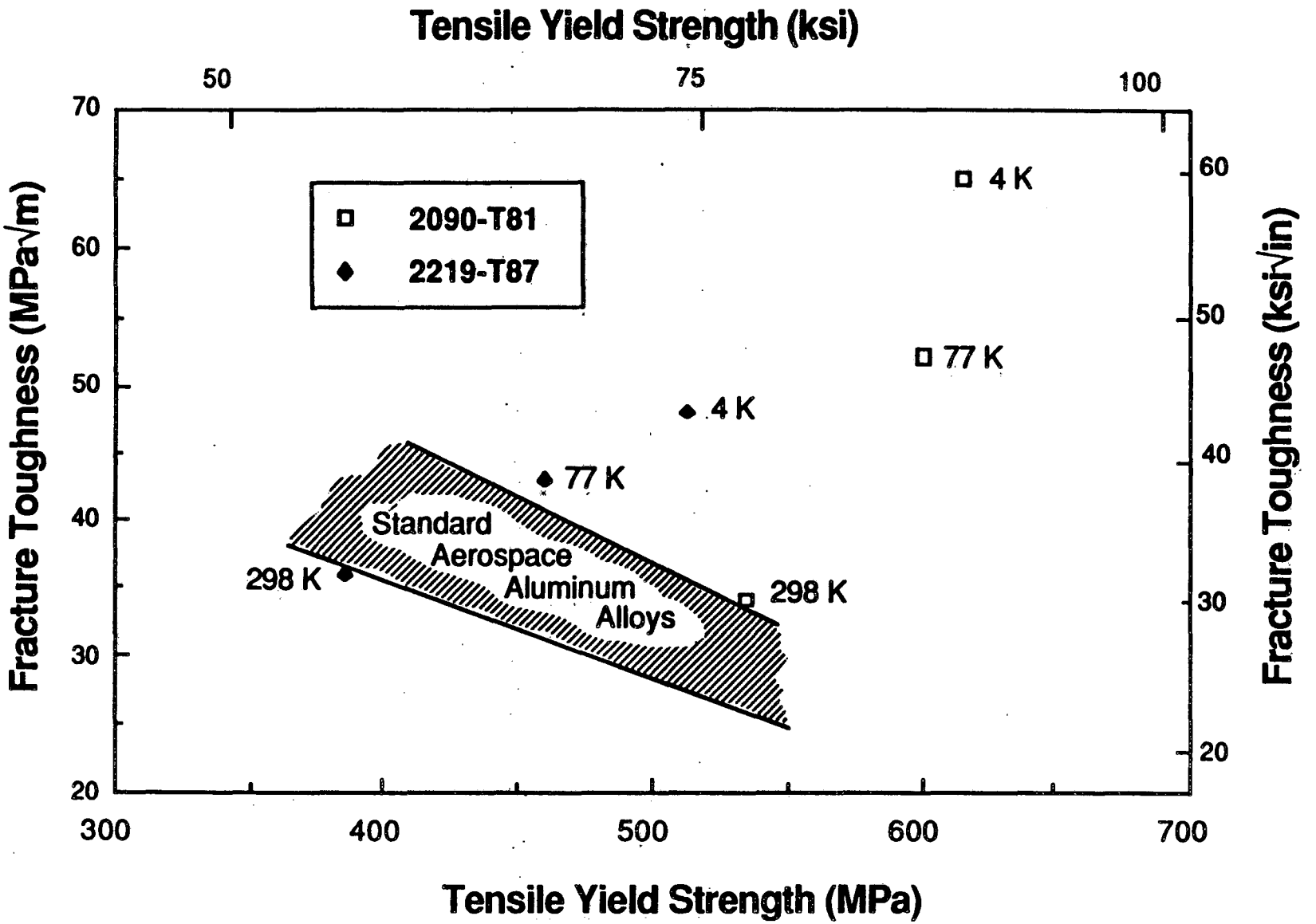

Figure 1. Yield strength- fracture toughness combination as a function of temperature for 2090-T81 alloy. The hatched region represents the range of strength-toughness combinations for typical aerospace aluminum alloys. Data for alloy 2219-T87 as a function of temperature are shown for comparison. (After ref. 1)

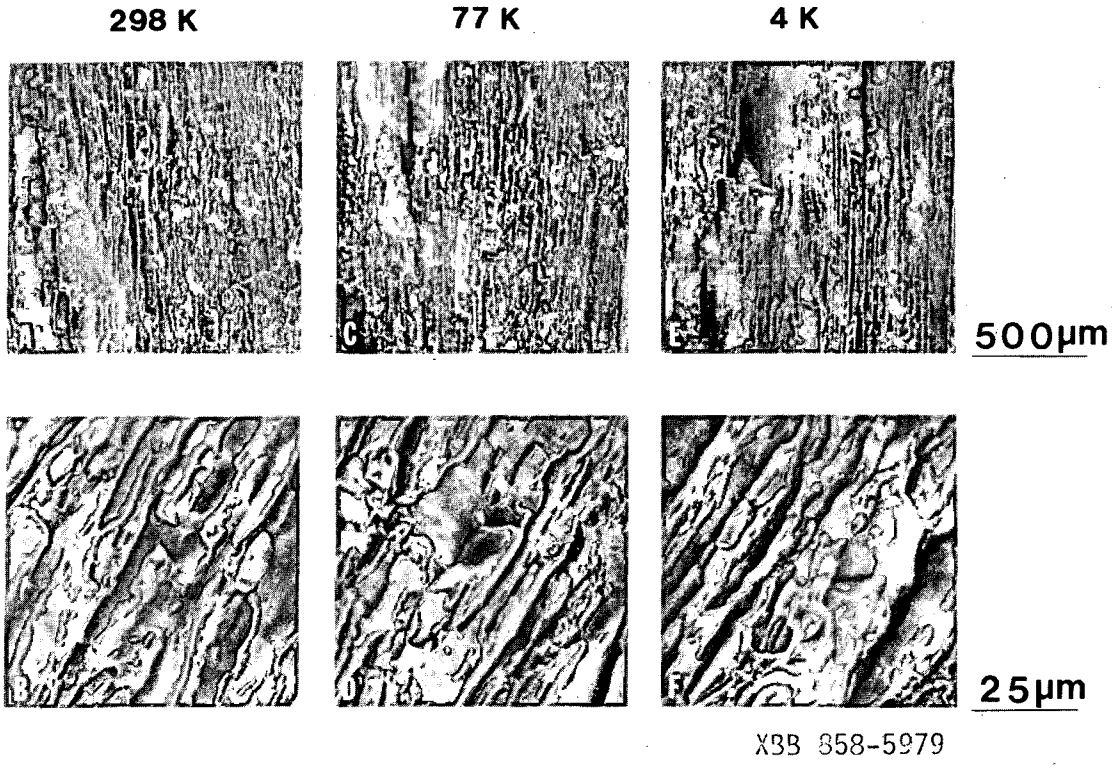

Figure 2. Scanning electron micrographs of fracture surfaces of J_{Ic} specimens broken at each test temperature. Note that the fracture mode appears to be unchanged. (From ref. 1)
XBB 858-5979

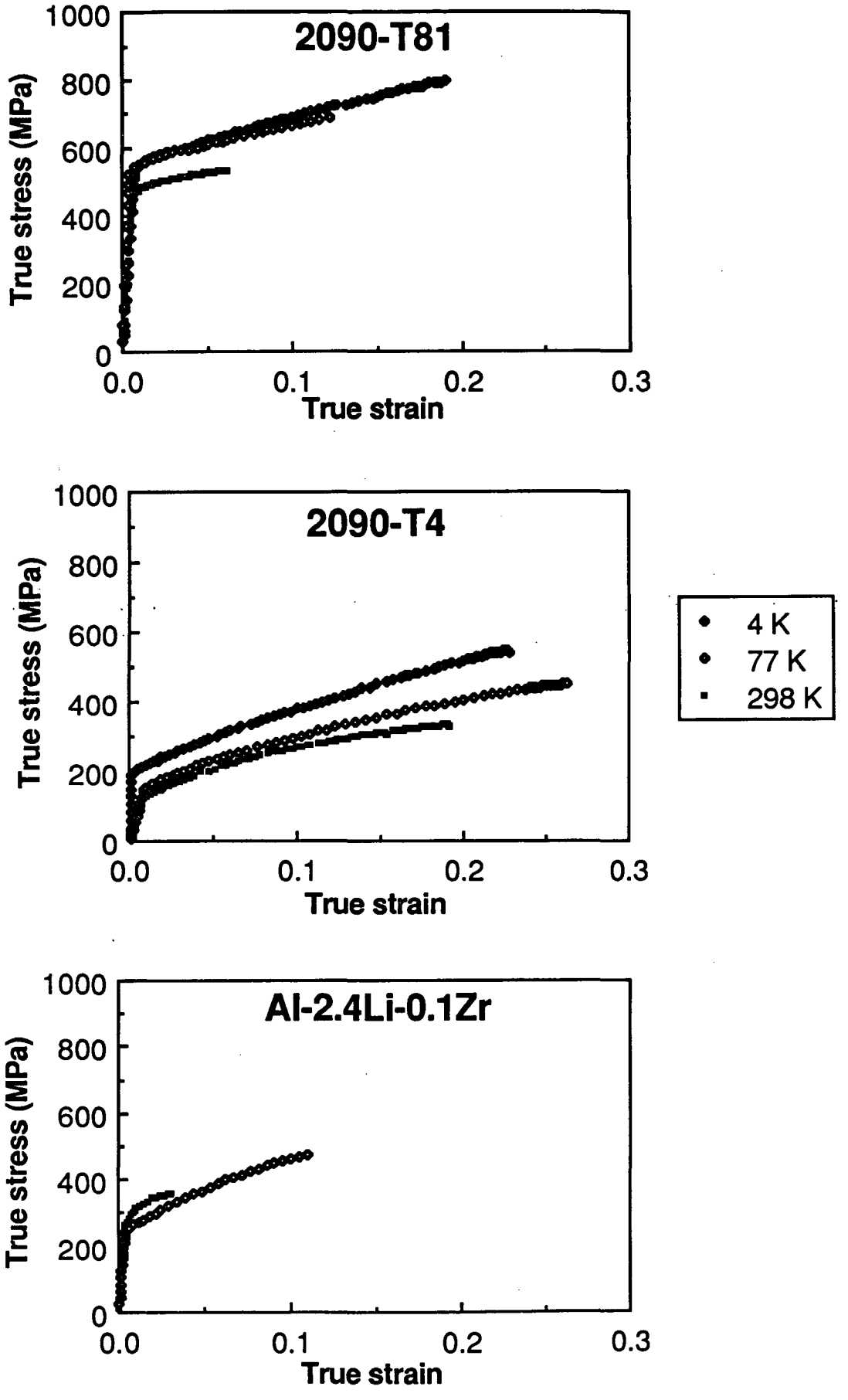

Figure 3. Effect of temperature on true stress-true strain curves for the three materials.

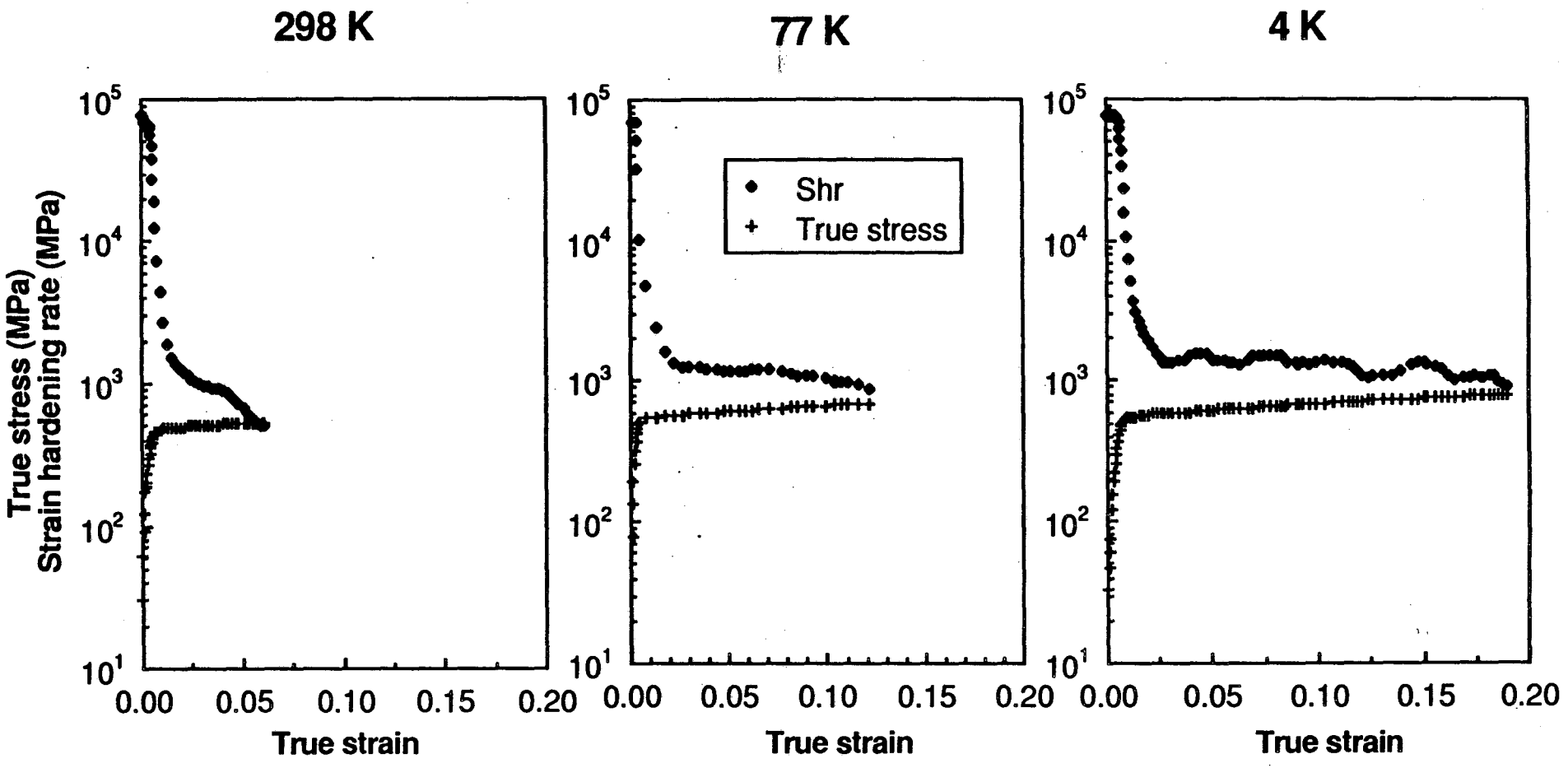

Figure 4. True stress and strain hardening rate (shr) plotted as a function of true strain for alloy 2090-T81 for each test temperature. The true stress and the strain hardening rate (both plotted on the vertical axis) are measured in the same units.

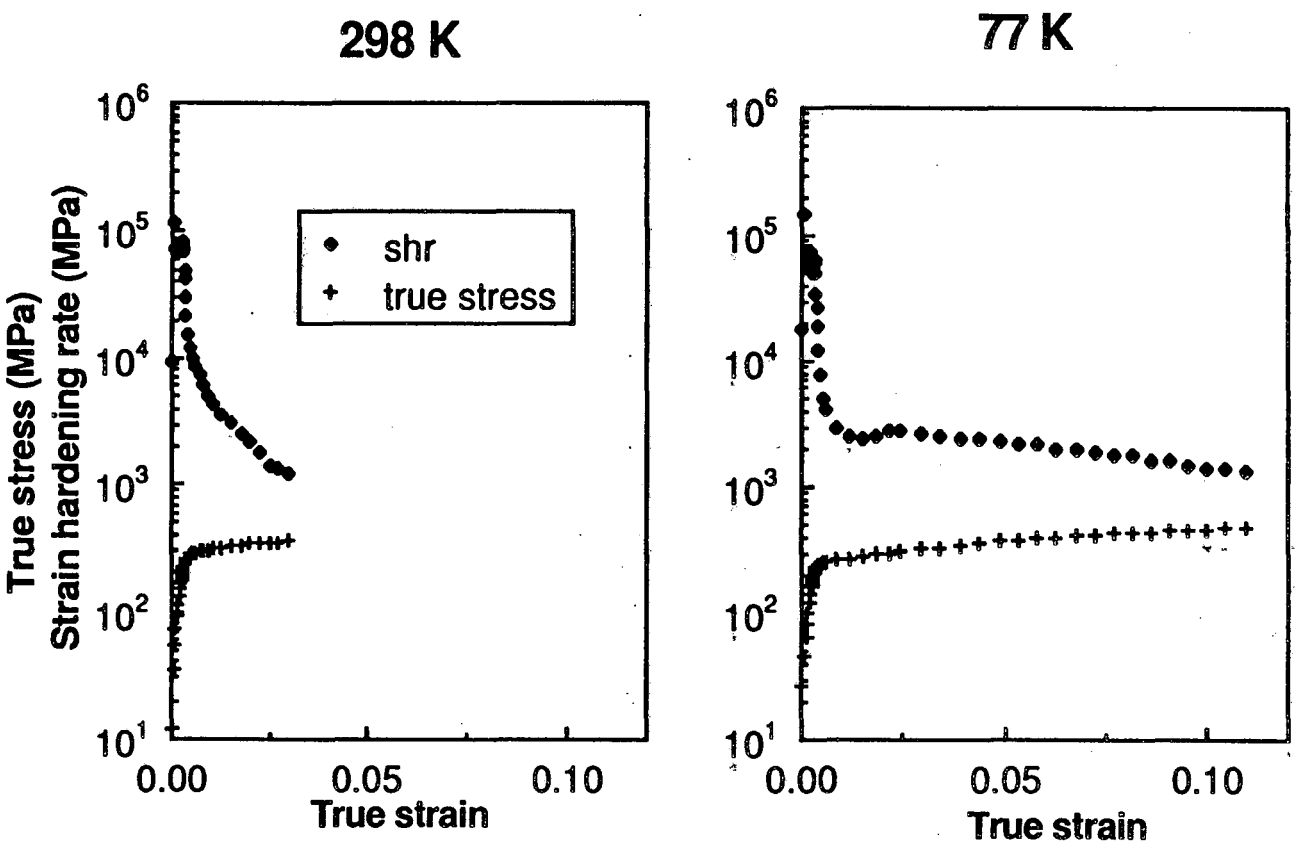

Figure 5. True stress and strain hardening rate (shr) plotted as a function of true strain for Al-2.4Li-0.1Zr alloy as a function of temperature.

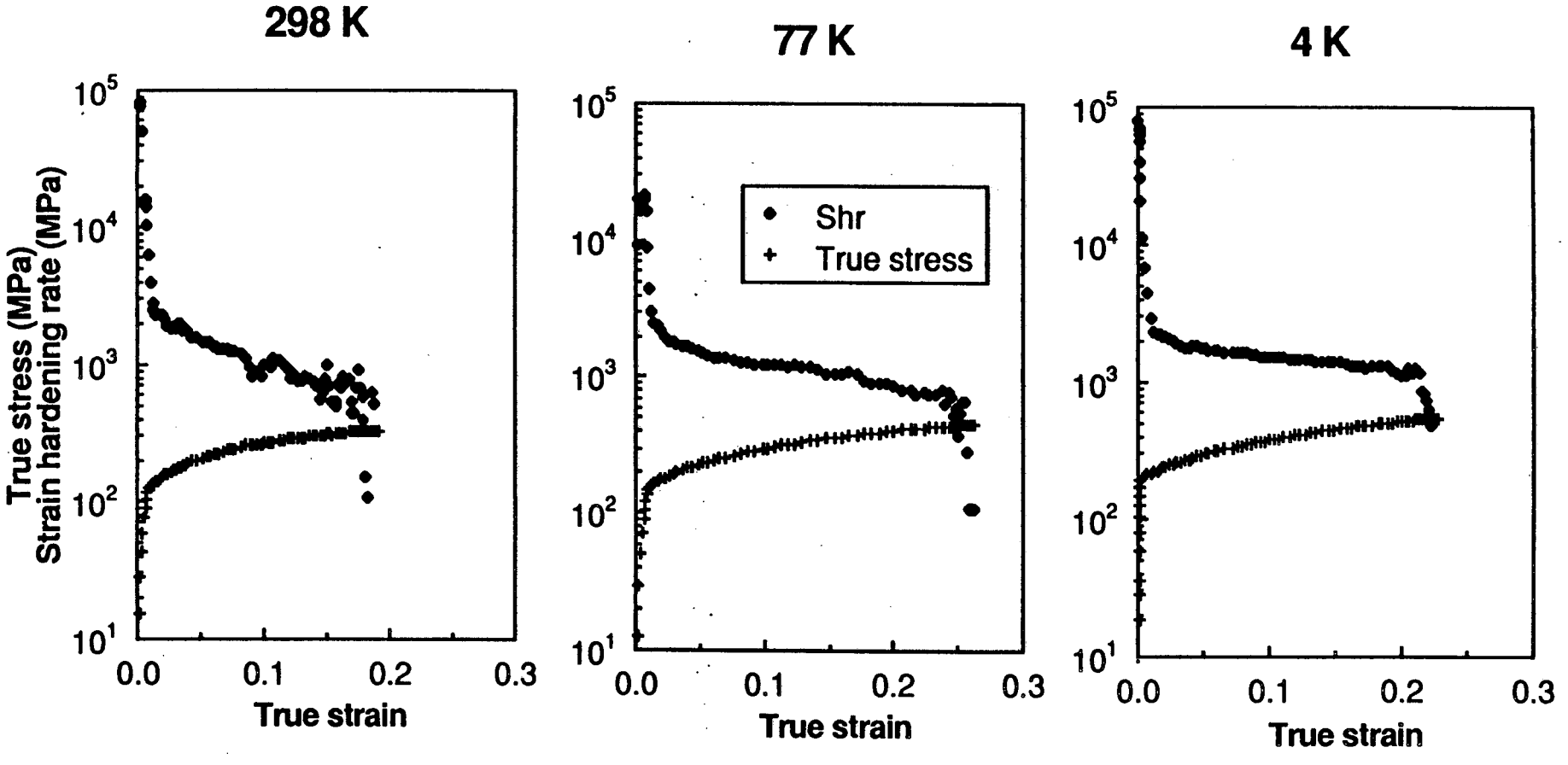

Figure 6. True stress and strain hardening rate (shr) plotted as a function of true strain for alloy 2090-T4 for each test temperature.

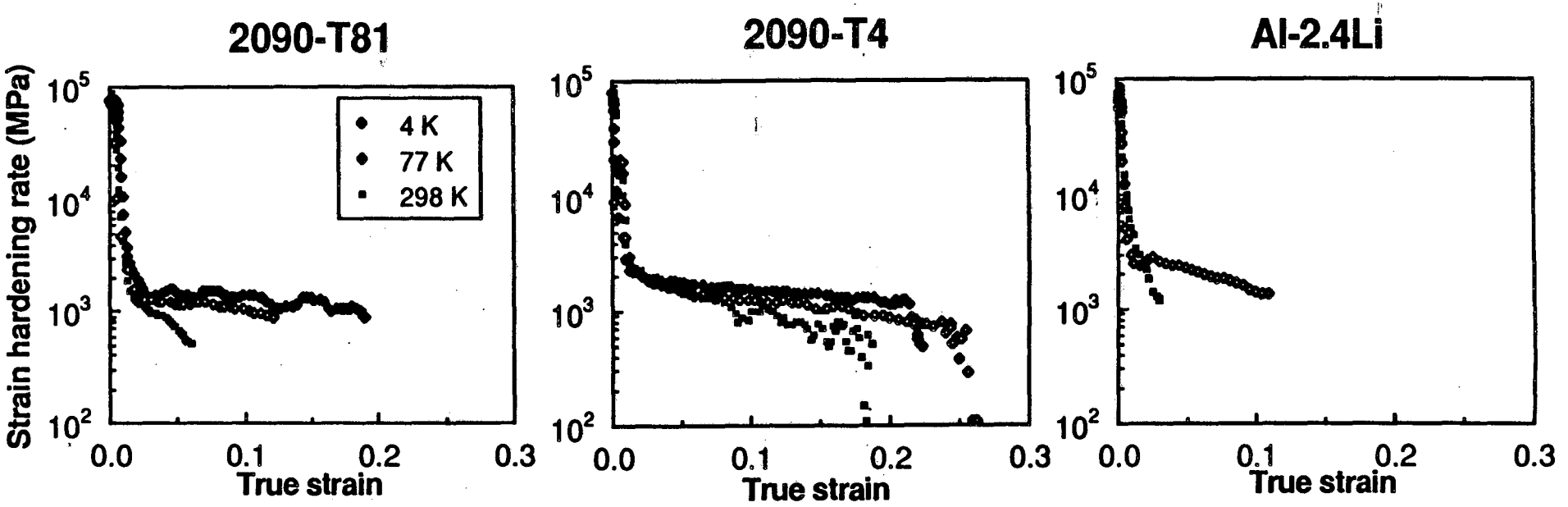

Figure 7. Effect of temperature on strain hardening rate plotted as a function of true strain for the three materials.

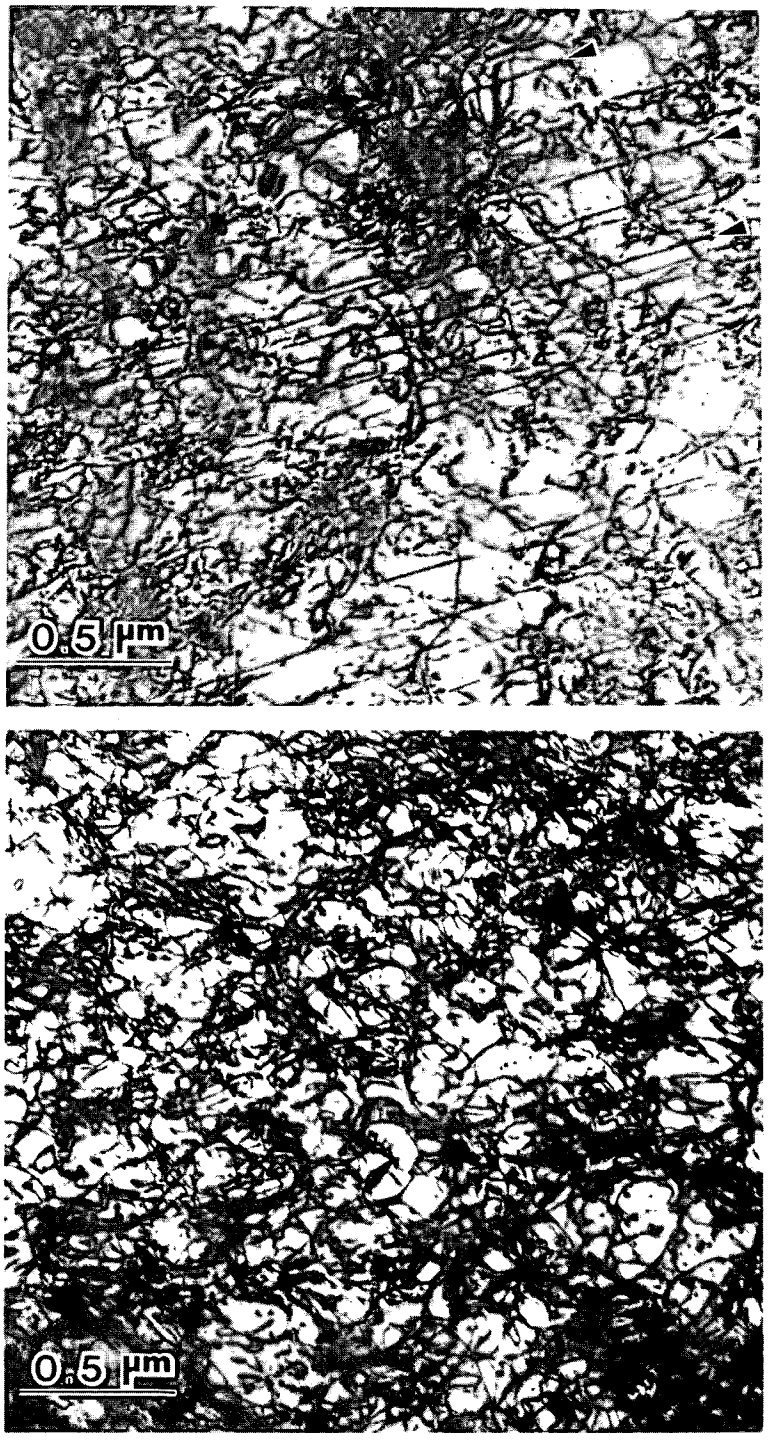

XBB 868-7421A

Figure 8. Transmission electron micrograph of alloy 2090-T4 deformed 8% in tension (top) at room temperature, (bottom) at 77 K. Examples of planar slip are arrowed in the upper micrograph. XBB 869-7421A

LAWRENCE BERKELEY LABORATORY
TECHNICAL INFORMATION DEPARTMENT
UNIVERSITY OF CALIFORNIA
BERKELEY, CALIFORNIA 94720